Flip-chip-integrated silicon nitride ECL at 640 nm with relaxed alignment tolerances

Ines Kluge[1], Michael Schulten[1], Alireza Tabatabaei Mashayekh[1], Rebecca Rodrigo[1], Manuel Ackermann[1], Ibrahim Ghannam[1], Andim Stassen[2], Florian Merget[1], Patrick Leisching[3], and Jeremy Witzens[1]

[1]Institute of Integrated Photonics, RWTH Aachen University, Campus Boulevard 73, 52074 Aachen, Germany
[2]imec, Kapeldreef 75, 3001 Leuven, Belgium
[3]TOPTICA Photonics, Lochhamer Schlag 19, 82166 Graefelfing, Germany

ABSTRACT

We present work towards a visible wavelength tuneable external cavity laser (ECL) on a silicon nitride platform working around 640 nm. A ring resonator Vernier structure on the photonic integrated circuit (PIC) provides delayed feedback with spectral filtering and tuning. Gain is provided by a reflective semiconductor optical amplifier (SOA) grown on a GaAs substrate and integrated by pick-and-place flip-chip assembly. In a novel coupling scheme, the 1-dB in-plane placement tolerance is relaxed by a multi-mode edge-coupler to ± 2.6 µm in the direction parallel to the SOA edge and to displacements up to 3.5 µm from the PIC interface along the SOA's optical axis. Pedestals defined in the PIC guarantee vertical alignment.

Keywords: Silicon nitride photonics, flip-chip assembly, hybrid integration, semiconductor lasers, semiconductor optical amplifier

1. INTRODUCTION

The integration of lasers into silicon chips has been an ongoing research topic since silicon photonics (SiP) emerged. There are several options to realise lasers on a silicon platform, which rely on other material systems, due to silicon's indirect bandgap. Monolithic integration of III-V or II-VI compound semiconductors provides direct bandgap materials as commonly used for laser diodes. Direct growth onto silicon is a conceptually attractive approach. However, it poses significant challenges, since mismatch in lattice constants and thermal expansion coefficients between most compound semiconductors and silicon will lead to defects and strain at the heterojunction.[1] Moreover, anti-phase-domains have to be prevented or managed. As a CMOS processing compatible alternative, group IV gain materials based on the silicon-germanium-tin (SiGeSn) system are also being very actively investigated,[2] however important challenges remain related to achievable alloy compositions and material quality.[3] Heterogeneous integration of compound semiconductors via wafer bonding,[4] on the other hand, has already reached commercial maturity.

Another option relies on hybrid integration of prefabricated laser dies or optical amplifiers with a SiP photonic integrated circuit (PIC). In some commercial solutions, such hybrid integration is facilitated by first mounting the laser in a micro-package,[5] that can enable isolation and active alignment.[6] Further research efforts aim at hybrid III-V chip integration without requiring a dedicated micro-package, among them flip-chip integration[7–10] as well as laser integration via photonic wire bonds.[11,12] Flip-chip integration in particular has the potential for being a very high throughput integration scheme. However, difficulties then arise in maintaining a good coupling efficiency, since it is not readily compatible with active alignment and obtaining good mode matching between the III-V chip and SiP PIC can be challenging without interposed optics. The placement accuracy of pick-and-place flip-chip bonders significantly improved over the last years and state-of-the-art equipment provides a placement accuracy of ±0.3 µm at 3σ. However, standard edge couplers already lose 1 dB at ±0.4 µm in-plane displacements for the 640 nm SOA that we aim to integrate.

Ines Kluge: E-mail: ikluge@iph.rwth-aachen.de

Silicon Photonics XVII, edited by Graham T. Reed, Andrew P. Knights, Proc. of SPIE Vol. 12006, 120060E · © The Authors. Published under a Creative Commons Attribution CC-BY 3.0 License · doi: 10.1117/12.2607615

Previous work has shown the realisation of hybridly integrated external cavity lasers (ECLs) at visible[13] and infrared[14] wavelengths using semiconductor optical amplifiers (SOAs) as external gain medium. However, in these a very precise alignment is needed. One possibility to address this is to very substantially expand the optical field on both sides of the optical interface by using delocalised modes in the III-V chip[15] and a low field confinement in the PIC platform.[16]

We use a different approach that does not require reengineering of the III-V gain material, but rather focuses on a smart interface on the PIC side in the form of alignment tolerant edge couplers that relax the requirements on the placement accuracy. These were first demonstrated by Romero-García et. al. in silicon for infrared light and have proven to increase the alignment tolerance along the in-plane axes by a factor 3 compared to standard edge couplers optimized for the same injected beam profile.[17] This is achieved by using a multi-mode interface and allowing the ground- and first-order modes to propagate in the coupler prior to equally splitting the light into two single mode waveguides, that are further used as part of a wavelength-selective Sagnac loop in the following. Its applicability to hybrid ECLs has been shown in the infrared spectral range.[18]

While early work on hybrid ECL integration has been mostly driven by the requirements of coherent communications, there is a growing need for short wavelength ECLs for various types of instrumentation. These include the field of bio- and life-sciences, e.g. for flow cytometry, fluorescence microscopy or optical coherence tomography (OCT), in which bulky and expensive lasers are still dominating,[19] as well as atomic clocks.[20] To realise hybridly integrated ECLs at such a short 640 nm wavelength, we have adapted this ECL concept to a silicon nitride (SiN) PIC technology, selected for its wide transparency window covering most of the visible and of the near infrared range and flip-chip integrated custom-made reflective (R)SOAs grown on GaAs wafers.[21] This paper reports the design and characterization of the PIC in Section II as well as the flip-chip integration process in Section III. Due to the moderate gain of our custom RSOAs and the relatively high insertion losses due to a mode mismatch arising from a different than expected RSOA emission profile, a full laser has yet to be demonstrated and remains under development. However, this work validates the required components, in particular the operation of the alignment tolerant edge coupler at a visible wavelength.

2. PHOTONIC INTEGRATED CIRCUIT

A schematic of the PIC with the flip-chipped RSOA is shown in Fig. 1a. The PIC is realised in a modification of imec's BioPIX SiN technology with a fully etched 150 nm thick SiN waveguide layer deposited by plasma enhanced chemical vapour deposition (PECVD) and surrounded by a silicon dioxide cladding on a silicon substrate. Light from the RSOA is coupled via an alignment tolerant multi-mode edge coupler (MMEC) whose two output waveguides are looped back to each other via two serially coupled ring resonators. The overall photonic circuit forms a wavelength-selective Sagnac loop using the Vernier effect to increase the rings' effective free spectral range (FSR). These can be thermally tuned via integrated metal heaters, allowing for selection of the laser wavelength within the RSOA's gain bandwidth. A 25 µm deep cavity has been etched into the PIC where the RSOA is to be attached, with pedestals left on the PIC determining the vertical placement of the RSOA (Fig. 1b). Their height can be fabricated in a very precise way by using the SiN layer as a natural etch stop.[8] The utilized RSOA is based on a tensile strained multi-quantum-well gain material grown on a GaAs substrate and operating at the transverse magnetic (TM) polarisation, that was custom made for this purpose. It has an anti-reflective coating on the front side, at which the waveguide is also angled by 5.5° to reduce back-reflections from the facet. The angle of the MMEC has been adapted on the PIC accordingly, taking refraction into account. The RSOA is provided with a high-reflectivity coating on its back-side and has a peak amplification at 639 nm. At locations corresponding to the six pedestals on the PIC, cavities have been etched into the RSOA that also stop close to the waveguide layer based on a chemical etch stop to ensure proper vertical alignment.

2.1 Vernier Structure

Ring resonators arranged in a Vernier structure are commonly used for the implementation of external cavity lasers.[14,22] By choosing two slightly different ring radii of 39 µm and 40 µm, the FSRs of the two rings, which are each close to 0.95 nm, are slightly detuned. Resonances then overlap at much larger intervals, extending the effective FSR of the whole device to about 40 nm. The resonance wavelengths of each of the rings are independently tunable by means of metal heaters placed on top of the rings excluding the waveguide junctions

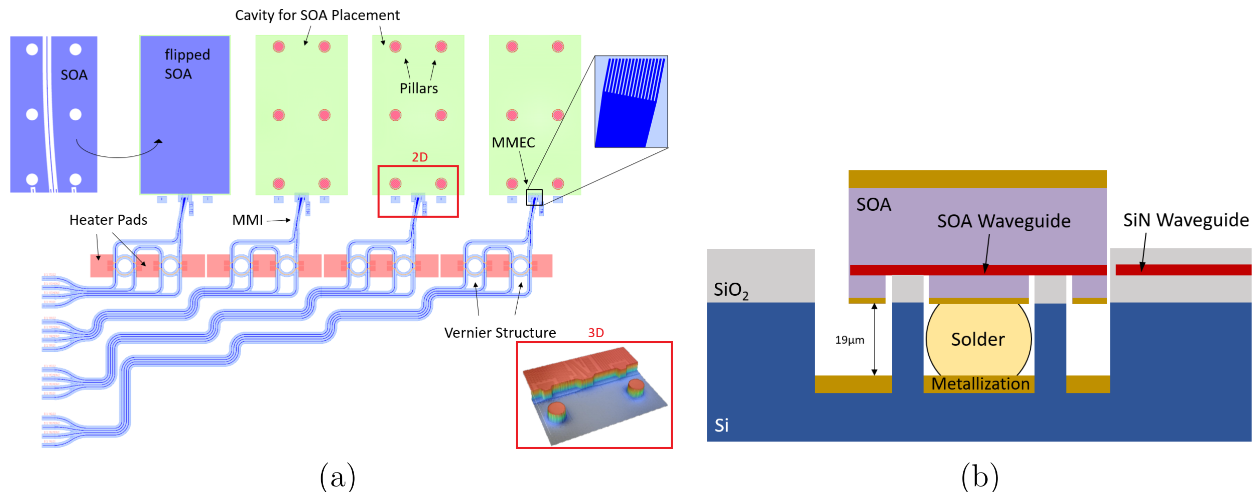

(a) (b)

Figure 1: PIC layout and RSOA integration concept. (a) PIC layout displaying four ECL structures with different parameters. An RSOA can be flipped onto each of the four cavities. (b) Side view of the PIC illustrating the integration concept for the RSOA. It is placed on pedestals left unetched in the PIC cavity.

Table 1: Measured ring characteristics for different ring gaps.

Ring Gap/µm	FWHM/pm	Q-factor	IL/dB	ER/dB	Max. Feedback/dB
0.36/0.30	58.7	10865	-5.1	-4.2	-10.2
0.44/0.39	45.3	14240	-11.1	-2.7	-22.3
0.49/0.45	34.8	18390	-15.4	-2.0	-31.8
0.52/0.49	33.6	19206	-17.7	-1.9	-35.9
0.54/0.52	28.8	22307	-17.0	-1.5	-35.0
0.55/0.55	23.1	29131	-17.2	-1.2	-34.5

and that cover about 75% of their circumference. Tuning over an entire FSR is possible for each ring by applying a current in the order of 20 mA and a total power of 170 mW. The waveguides are 600 nm wide. Gaps between the ring and bus waveguides vary between 0.3 µm and 0.55 µm depending on the chosen design.

Measurements were performed on the individual rings that have a full width at half maximum (FWHM) between 59 pm and 23 pm, a loaded quality (Q-)factor between 11000 and 29000, an extinction ratio (ER) between −4.2 dB and −1.2 dB and insertion losses (ILs), measured between drop and bus waveguide, between −5.1 dB and −17.2 dB. This data has been summarised in Tab. 1. The ring gaps refer to the through and drop port gap of the respective ring.

As expected, the Q-factor and IL increase with increasing gap sizes as a consequence of the reduced coupling strength. The minimum ILs of 5.1 dB are rather high as the light has to transit through two rings and is thus attenuated by over 10 dB, in addition to interface losses, prior to returning to the RSOA. They are partially due to the finite ER of the rings, and thus to the light outcoupling from the laser, as well as to waveguide losses inside the rings. From this data, we could fit waveguide losses of 9.9 dB/cm. Given these, narrower gaps would have been preferable.

2.2 Alignment Tolerant Multi-Mode Edge Coupler

A generic schematic of the MMEC is shown in Fig. 2. For the device used here, light enters the structure through an array of 17 parallel waveguide tips spaced 500 nm center-to-center, each starting with a narrow 300 nm width. The interface is angled by 10.4° to account for the RSOA waveguide output angle. In total, the interface has a width of 8.44 µm. Since the light is weakly confined at the tips and their individual modes very strongly overlap, they form, together, the equivalent of a slab waveguide with an increased mode dimension in the vertical direction. They are first merged into an actual slab waveguide, that is then tapered down over a length of 75 µm to a width of 800 nm, corresponding to a waveguide that supports only two TM modes, the ground and

first order modes. The length of this section was also varied from device to device and needs to be such that the two excited modes acquire a π phase shift at the point were it is separated into two single mode waveguides by a Y-junction. Since they are then in quadrature, this results in equal power splitting even if the modes are excited with varying amplitudes due to lateral misalignment.[17,18] The second-order and even higher-order modes are rejected by the structure. The broadened input coupling section together with the coupling of both the ground and first order modes increases the misalignment tolerance in the in-plane directions, although this comes at the cost of a slightly lower coupling efficiency due to the increased number of transitions in the structure.

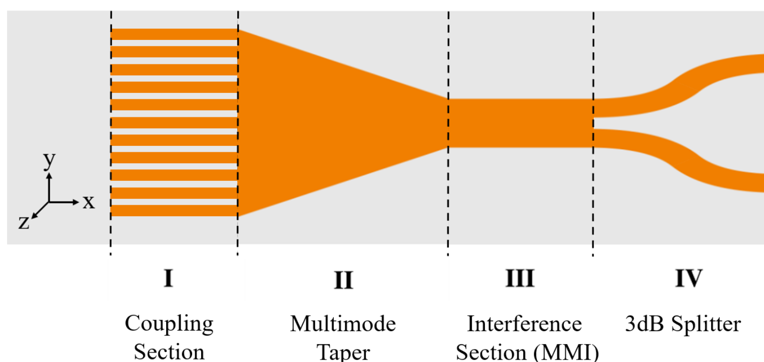

Figure 2: Schematic of the MMEC. The number of tips represented in the figure has been reduced for clarity.

Characterisation of the functionality of the MMEC was carried out on test devices with different interference section lengths. Light was coupled in by the RSOA and measured at the two single mode waveguides behind the Y-junction. In order to measure the alignment tolerances, these measurements were done in an opto-mechanical setup in which the RSOA was freely movable, as opposed to permanently attaching it to the PIC as done in Section III. The RSOA was moved in the lateral direction along the width of the coupling section. Depending on the length of the interference section, the power at the two outputs exhibits different characteristics (Fig. 3). When the MMEC is centred, the output power curves for the two waveguides coincide in all devices, as expected based on the symmetry of the structure. However, this is not necessarily true for off-centred RSOA positions, for which the symmetry is broken. Thus, when moving the RSOA laterally along the PIC interface, the power in one output rises, while it falls in the other. This indicates that the modes are not in quadrature (Fig. 3a-3c). With increasing interference section length, this characteristic however disappears, indicating that the structure approaches the targeted quadrature condition. At a length of 8.451 µm (Fig. 3d), the two output powers remain almost equal irrespective of the displacement and show almost equal power splitting. The 1- and 3-dB lateral alignment tolerances are defined here as the distance Δx at which the total power summed over both waveguides drops below 1 dB or 3 dB of the total power coupled at the centre position. The device with an MMI length of 8.451 µm, that is close to quadrature, has a maximum transmission of −13.8 dB and 1 dB/3 dB lateral (y-direction) misalignment tolerances of ±2.6 µm and ±3.8 µm. The alignment tolerances in the vertical (z) and in the axial in-plane (x) direction are defined analogously and have been determined to be ±1.1 µm/±1.9 µm in the vertical direction and 3.5 µm (1 dB) in the axial direction.

It has to be noted that the MMEC exhibits high coupling losses (Fig. 4a), other than previously published results in the near infrared for which commercial RSOAs with well known beam characteristics were used that could be designed for. Here, the losses originate primarily from the mismatch between the RSOA mode that was designed for and the one that was later experimentally obtained, as well as a mismatch in the assumed and experimental emission angles of the RSOA. Simulations of the MMEC give an MMEC supermode mode field diameter (MFD), given by the positions at which the field intensity drops to $1/e^2$, of 7.9 µm in the horizontal direction and 1.3 µm in the vertical direction, while the RSOA has an MFD of 1.16 µm in the horizontal and 2.2 µm in the vertical direction. Fig. 5 shows the mode profile of the RSOA determined from its measured far field beam shape, the simulated mode profile of the MMEC and their 2D overlap. When the RSOA is centred relative to the MMEC, this results in an insertion loss of −7.1 dB, that can be broken down into 0.6 dB due to MFD mismatch in the vertical direction, 5.4 dB due to MFD mismatch in the horizontal dimension and an additional 1.1 dB due to the MMEC interface not behaving exactly like a slab waveguide, i.e., the small-structure in the MMEC modes

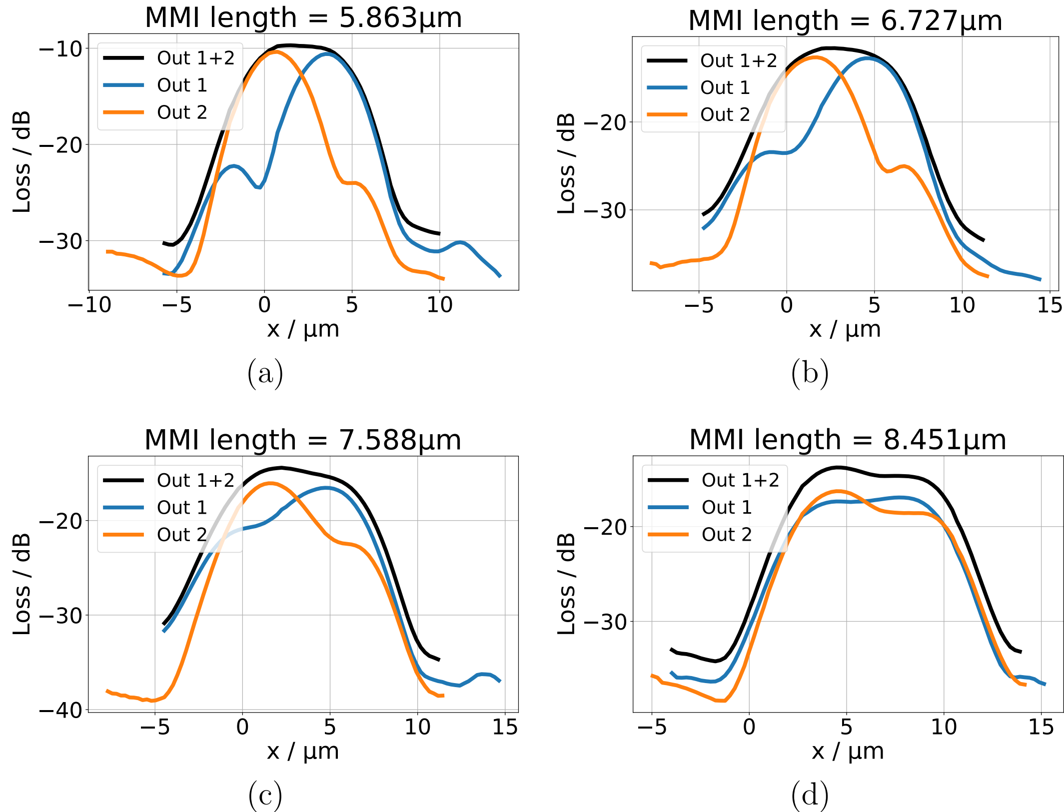

Figure 3: Measurement of MMEC test structures. Depending on the length of the interference section, the respective output power levels exhibit different characteristics. (a) to (d) show the transition from a device far from quadrature to one almost fully in quadrature.

reflecting the periodicity of the array of waveguide tips. The insertion losses due to mismatch in the vertical direction could be improved by reducing the tip widths, further reducing the field confinement on the MMEC side, as verified by simulations in the following.

It is typical for MMECs to have an in-plane MFD that is somewhat larger than that of the beam they are receiving, since this improves the misalignment tolerance while at the same time some of the losses resulting from mode mismatch are recovered at lateral displacements, once the 1st order mode is also excited. As seen in Fig. 3d, at small lateral misalignments, the insertion losses are actually better than for the centred position. In an optimised structure, the coupling efficiency for a centred RSOA should be allowed to drop up to 1 dB from the maximum at lateral displacements, since this does not penalise the misalignment range in which a 1-dB IL penalty is obtained relative to the maximum. In typical designs, the in-plane MFD of the MMEC is about 50% wider than that of the RSOA or other coupled to device.[17,18] Here, the in-plane MFD of the MMEC is however excessively large compared to that of the RSOA.

The expected 3-dB misalignment tolerance from the simulation is $\pm 3.6\,\mu m$ in the y-direction and $\pm 0.7\,\mu m$ in the z-direction, which matches the measured misalignment tolerances (Fig. 4b).

A comparison of the emission/acceptance angles of the two devices also showed a deviation of a few degrees. The RSOA's emission angle is 14.9°, while that of the MMEC is measured to be 18.2°. Calculations with a tilted Gaussian show that a deviation of 3.3° already results in a loss of about 3 dB. The total ILs seen in the device characterisation are thus well accounted for by simulations, once the experimental RSOA characteristics are considered. Even though the MMEC has been designed for different RSOA characteristics, with a different MFD and emission angle, the targeted MMEC functionality is obtained as expected.

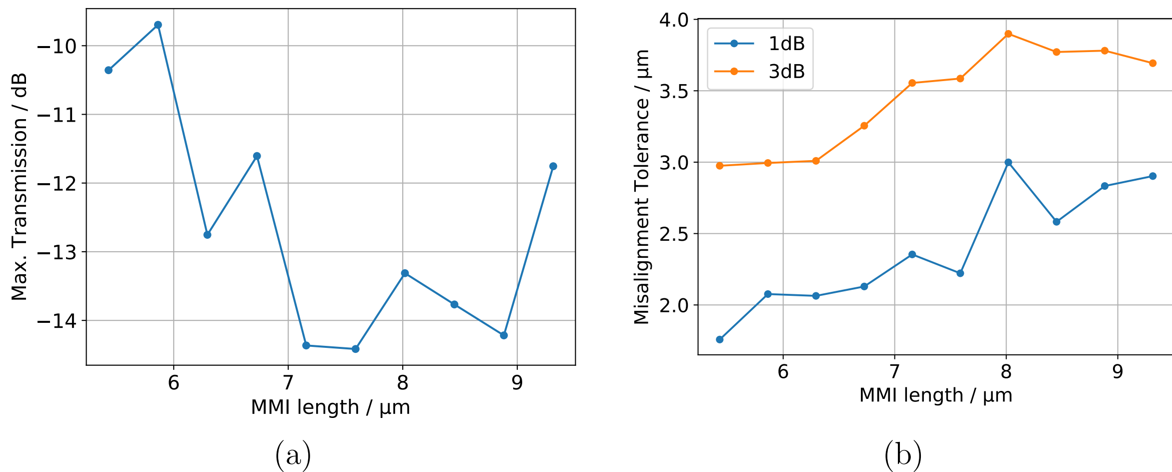

Figure 4: MMEC test structure characteristics for different multimode interference section (MMI) lengths. (a) Peak coupling efficiency and (b) lateral misalignment tolerance along the edge of the PIC interface (y-direction).

To evaluate how a MMEC would operate if it was tailored to the RSOA's characteristics, we performed simulations in which the number of waveguides in the coupling section and the width and distance between them were swept. A device with an array of 5 waveguides, a tip width of 0.2 µm and a waveguide-to-waveguide distance of 0.35 µm would allow for a placement tolerance of ± 1.37 µm (1 dB) in the horizontal direction while maintaining a centred coupling efficiency of -2.6 dB. This corresponds to an improvement by a factor 3 compared to a standard edge coupler with a placement tolerance of ± 0.42 µm (1 dB).

3. EXTERNAL CAVITY LASER AND FLIP-CHIP ASSEMBLY

For flip-chip assembly, the bottom of the cavity on the PIC has to be metallized for bottom electrode functionality. A layer stack of 50 nm Ti / 800 nm Ni / 50 nm Ti / 150 nm Au was selectively deposited using electron beam evaporation and a lift-off process. For soldering, the chips were prepared with 40 µm diameter AuSn solder bumps solder jetted onto the contact pads prior to assembly (Fig. 6a). The Ti/Ni/Ti/Au layers act as under-bump metallization for the solder balls. The small ball diameter enables versatile patterns and multi-ball stacking and is compatible with the small size of the RSOA. The large number of jetted solder balls also serves to ensure sufficient heat sinking.

Previous attempts using solder paste with a rotary dispensing system did not yield reproducible results, due to the difficulty of dispensing it in the small area of the cavity while avoiding the pedestals. Using the required solder paste with very small metal particles also proved challenging in terms of obtaining a sufficiently good electrical contact. As an effect of changing environmental factors and possibly inhomogeneity in the composition of the solder paste itself, the required solder dot size of 400 µm was not achieved in a reproducible way and this approach was not further pursued.

The flip-chip process with a face-down attachment of the RSOA was performed with an Amicra NANO die bonder. The process consists in a sequence of alignment, handling and soldering steps, in which the system is able to handle and recognise chips automatically on the basis of recurring patterns with an image processing software. This way, a high placement accuracy before and after soldering can be ensured. The soldering of the AuSn solder balls is performed using a 100 W laser at 30% power for 7 s which is applied from underneath the PIC over a circular area of 400 µm diameter, which corresponds exactly to the width of the RSOA. During the soldering process, the PIC is held in position by a vacuum holder, while the RSOA is still attached to the bond tool. The high precision process yields an alignment accuracy below 2 µm after soldering, which could be improved further by using compliant alignment markers to reach the requirements of the redesigned MMECs.

Since this process still remains under development, an earlier result obtained with solder paste attachment is shown in Fig. 6b. Light can be seen to be coupled from the SOA into the SiN PIC. In particular, the two bright

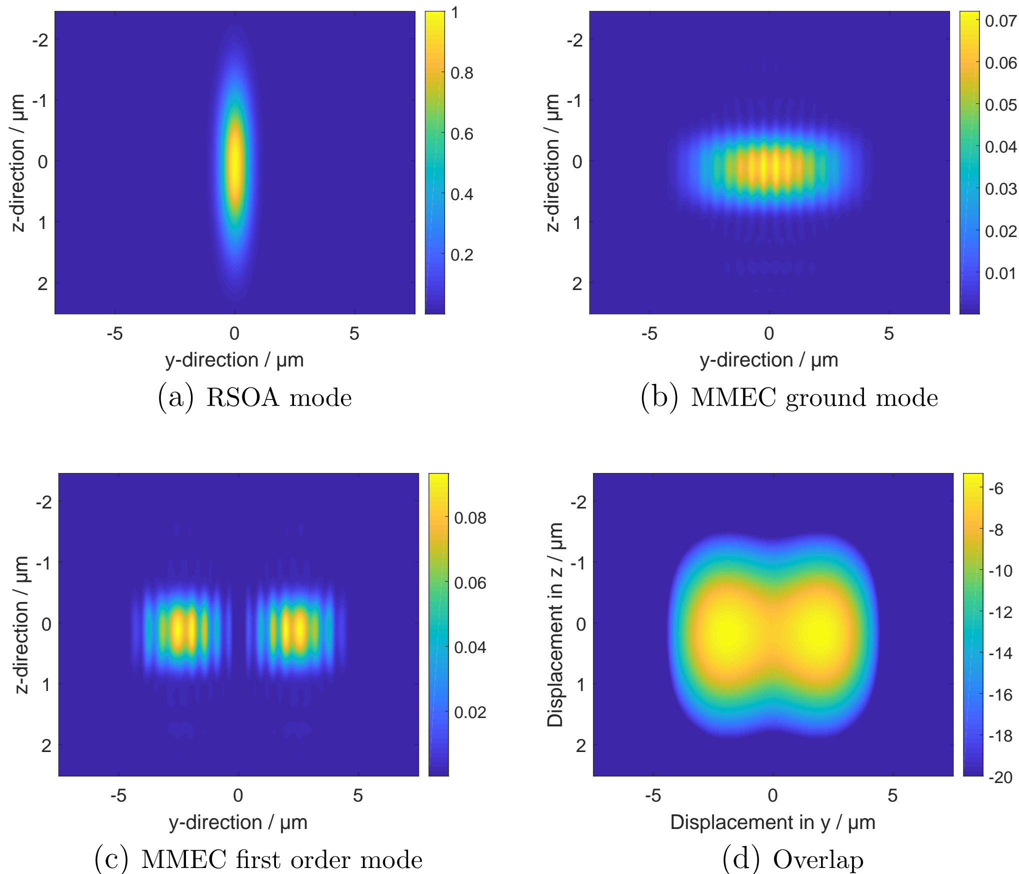

Figure 5: RSOA and MMEC modes and their overlap. The RSOA mode, approximated as a Gaussian beam, was determined from its far field emission pattern. MMEC modes are obtained from simulations. In (d), the overlap of the RSOA mode was taken with the simulated ground- and first-order MMEC modes. The axis labelling is identical to that in Fig. 2.

spots on the right side of the PIC correspond to the output ports of the two coupled-to waveguides at the output of the MMEC. However, lasing operation could not yet be achieved due to the high round trip losses in the order of 30 dB in this first PIC design.

4. CONCLUSION

In this work, we describe an integration concept for an ECL operating in the visible spectral range, that makes use of relaxed alignment tolerances provided by a multi-mode edge coupler. A high-volume manufacturing compatible and high-precision flip-chip bonder implements pick-and-place assembly of the RSOA onto the PIC. The presented MMEC works as expected and splits the coupled power evenly into its two single-mode output waveguides, even at significant lateral misalignment. However, a mismatch in the designed for and experimentally obtained RSOA emission characteristics created significant insertion losses currently precluding lasing. A flip-chip assembly proces using the high-accuracy flip-chip bonder in combination with solder ball jetting is under development, with first promising results. A placement accuracy of less than 2 µm was achieved, close to the required tolerances to fabricate this device. Simulations show that a redesign of the MMEC would result in significantly reduced coupling losses of −2.6 dB, while maintaining a misalignment tolerance of ±1.37 µm.

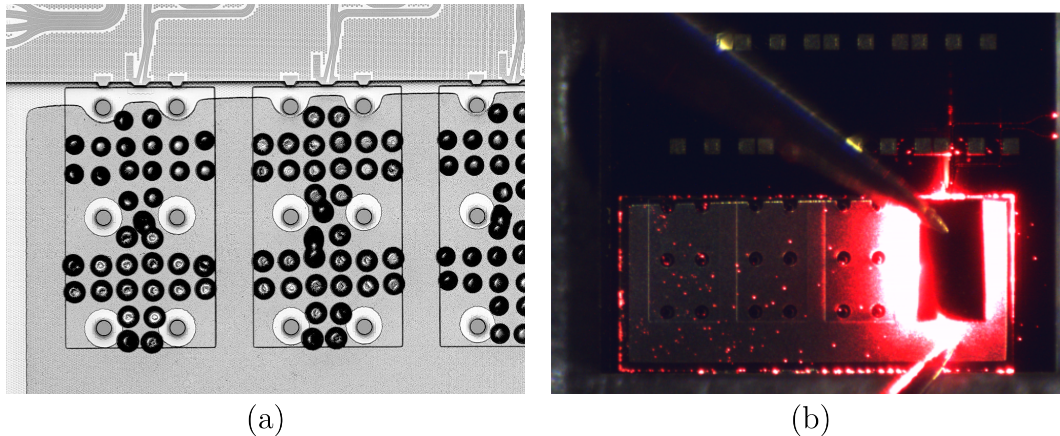

(a) (b)

Figure 6: Flip-chip process. (a) Laser scanning image of ball bonds jetted on the metallized PIC cavity. (b) Photograph of the PIC with a flip-chipped RSOA that is current injected with probe tips.

ACKNOWLEDGMENTS

The authors would like to acknowledge funding from the European Union under project PIX4life (688519) and from the German Federal Ministry of Education and Research for project HiPEQ (13N15965).

REFERENCES

[1] Tang, M., Park, J.-S., Wang, Z., Chen, S., Jurczak, P., Seeds, A., and Liu, H., "Integration of iii-v lasers on si for si photonics," *Progr. in Quant. Electron.* **66**, 1–18 (2019).

[2] Moutanabbir, O., Assali, S., Gong, X., O'Reilly, E., Broderick, C., Marzban, B., Witzens, J., Du, W., Yu, S.-Q., Chelnokov, A., Buca, D., and Nam, D., "Monolithic infrared silicon photonics: The rise of (si)gesn semiconductors," *Appl. Phys. Lett.* **118**, 110502 (2021).

[3] Marzban, B., Stange, D., Rainko, D., Ikonic, Z., Buca, D., and Witzens, J., "Modeling of a sigesn quantum well laser," *Photon. Res.* **9**, 1234–1254 (2021).

[4] Komljenovic, T., Huang, D., Pintus, P., Tran, M. A., Davenport, M. L., and Bowers, J. E., "Photonic integrated circuits using heterogeneous integration on silicon," *Proceedings of the IEEE* **106**, 2246–2257 (2018).

[5] Narasimha, A. et al., "An ultra low power cmos photonics technology platform for h/s optoelectronic transceivers at less than $1 per gbps," *in Proc. Opt. Fib. Comm. Conf. (OFC)*, OMV4 (2010).

[6] Snyder, B., Corbett, B., and O'Brien, P., "Hybrid integration of the wavelength-tunable laser with a silicon photonic integrated circuit," *J. Lightw. Technol.* **31**, 3934–3942 (2013).

[7] Tanaka, S., Jeong, S.-H., Shigeaki, S., Kurahashi, T., Tanaka, Y., and Morito, K., "High-output-power, single wavelength silicon hybrid laser using precise flip-chip bonding technology," *Opt. Expr.* **20**, 28057–28069 (2012).

[8] Moscoso-Mártir, A. et al., "Hybrid silicon photonics flip-chip laser integration with vertical self-alignment," *in Proc. Conf. on Las. and Electro-Opt. Pacific Rim (CLEO-PR)*, s2069 (2017).

[9] Matsumoto, T. et al., "Hybrid-integration of soa on silicon photonics platform based on flip-chip bonding," *J. Lightw. Technol.* **37**, 307–313 (2019).

[10] Mitchell, C. J., Li, K., Schachler, R., Khokhar, A., Chen, X., Stankovic, S., Wang, X., Sessions, N. P., Grabska, K. M., Thomson, D. J., Daedlow, C., Reed, G. T., and Wilkinson, J. S., "Tooling and procedures for hybrid integration of lasers by flip-chip technology," *in Proc. 8th IEEE Electron. Sys.-Integr. Technol. Conf. (ESTC)*, 1–7 (2020).

[11] Blaicher, M. et al., "Hybrid multi-chip assembly of optical communication engines by in situ 3d nano-lithography," *Light: Sci. and Appl.* **9**, 71 (2020).

[12] Xu, Y. et al., "Hybrid external-cavity lasers (ecl) using photonic wire bonds as coupling elements," *Sci. Rep.* **11**, 16426 (2021).

[13] Franken, C. A. A., van Rees, A., Winkler, L. V., Fan, Y., Geskus, D., Dekker, R., Geuzebroek, D. H., Fallnich, C., van der Slot, P. J. M., and Boller, K.-J., "A hybrid-integrated diode laser in the visible spectral range," *Opt. Lett.* **46**, 4904–4907 (2021).

[14] Fan, Y., van Rees, A., van der Slot, P. J. M., Mak, J., Oldenbeuving, R., Hoekman, M., Geskus, D., Roeloffzen, C. G. H., and Boller, K.-J., "Hybrid integrated inp-si_3n_4 diode laser with a 40-hz intrinsic linewidth," *Opt. Expr.* **28**(15), 21713–21728 (2020).

[15] Faugeron, M. et al., "High peak power, narrow rf linewidth asymmetrical cladding quantum-dash mode-locked laser," *J. Sel. Top. Quant. Electron.* **19**, 1101008 (2013).

[16] Blumenthal, D. J., Heideman, R., Geuzebroek, D., Leinse, A., and Roeloffzen, C., "Silicon nitride in silicon photonics," *Proceedings of the IEEE* **106**(12), 2209–2231 (2018).

[17] Romero-García, S., Marzban, B., Merget, F., Shen, B., and Witzens, J., "Edge couplers with relaxed alignment tolerance for pick-and-place hybrid integration of iii–v lasers with soi waveguides," *J. Sel. Top. Quant. Electron.* **20**(4), 369–379 (2014).

[18] Ghannam, I., Shen, B., Merget, F., and Witzens, J., "Silicon nitride external cavity laser with alignment tolerant multi-mode rsoa-to-pic interface," *J. Sel. Top. Quant. Electron.* **28**, 1501710 (2022).

[19] Domenech, J. D., Porcel, M. A., Jans, H., Hoofman, R., Geuzebroek, D., Dumon, P., van der Vliet, M., Witzens, J., Bourguignon, E., Artundo, I., and Lagae, L., "Pix4life: photonic integrated circuits for bio-photonics," *in Proc. Europ. Conf. Int. Opt. (ECIO)* (2018).

[20] Loisel, J. P., Topsu, S., Chassagne, L., Alayli, Y., Dahoo, P. R., and Juncar, P., "Generation of 656 nm coherent red-light by frequency-doubled nd:$ylif_4/\beta$-bab_2o_4 laser for a compact silver atoms optical clock," *Int. J. Metrol. Qual. Eng.* **3**, 7–13 (2012).

[21] Shimada et al., "640-nm laser diode for small laser display," *Proc. SPIE* **7198**, 7198O6 (2009).

[22] Zhu, Y. and Zhu, L., "Narrow-linewidth, tunable external cavity dual-band diode lasers through inp/gaas-si3n4 hybrid integration," *Opt. Expr.* **27**, 2354–2362 (Feb 2019).